Soft fluidic actuator based on nylon artificial muscles

Engineering Research Express

PAPER

Soft fluidic actuator based on nylon artificial muscles

Lee Sutton and Carlo Menon

MENRVA Research Group, School of Engineering Science, Simon Fraser University, Burnaby, Canada

E-mail: carlo_menon@sfu.ca

Keywords: soft robotics, nylon, soft actuators

RECEIVED
23 May 2019

REVISED
21 June 2019

ACCEPTED FOR PUBLICATION
1 July 2019

PUBLISHED
25 July 2019

Abstract

Soft robots have become increasingly prevalent due to their distinct advantages over traditional rigid robots such as high deformability and good impact resistance. However, soft robotics are currently limited by bulky, non-portable methods of actuation. In this study, we propose an inflatable soft actuator driven by nylon artificial muscles. By utilizing nylon artificial muscles, the system does not require sizable pumps or compressors for actuation. The paper investigates the properties of the proposed soft actuation system both analytically and experimentally.

1. Introduction

One of the biggest challenges for soft robotics is the design of extendable, portable methods for actuation [1]. The segments of a soft robot are typically actuated in one of two ways: tendons of varying length may be embedded into the soft segments to achieve motion; or pneumatic actuation may be used to pressurize inflatable channels which cause the material to deform to the desired configuration [1]. Tendon systems typically rely on electric motors to contract. These electric motors produce high specific power outputs, but require transmission systems to perform non-repetitive tasks, which increases the size, and weight of the overall system [2]. Pneumatic actuators rely on external pressure sources that are generally limited to pumps, compressors, or cylinders of compressed air [3].

Biological muscles offer many advantages over electric motors and pneumatic actuation methods. Skeletal muscles can produce large forces under varying strains, exhibit fast actuation times, and have high power to-weight ratios [4]. Researchers in the field of artificial muscles aim to create an actuator that matches these desirable properties. Some of the technologies currently being examined include piezoelectric polymers, shape memory alloys, ferroelectric dielectric elastomers, and polyelectrode gels [2, 5–7]. These materials deform when an chemical, electrical, or thermal stress is applied [8]. However, these technologies suffer from certain limitations such as low life cycle, hysteresis, high voltage requirements, and low efficiency [2, 9, 10]. A muscle-like technology whose performance could match that of skeletal muscle would be beneficial for the field of soft robotics.

Haines *et al* recently discovered a new type of artificial muscles that match or exceed the performance of biological muscles [11]. These artificial muscles are produced by coiling nylon fibres. Nylon fibres are made up of polymer chains oriented in the fibre direction which undergo large revesrible contractions when heated. Haines *et al* showed that uncoiled nylon fibres can contract up to 4% when a thermal load is applied. They showed that the tensile stroke may be amplified by coiling the fibres to make them chiral. Depending on the coil parameters, the coiled fibres may contract up to 49%, exceeding skeletal muscles (20%) [11]. In addition, nylon actuators have been shown to generate power densities of up to 5.3 kW kg^{-1}, compared to 0.32 kW kg^{-1} for the average human skeletal muscle [9].

In this study, soft actuators are proposed which make use of nylon artificial muscles to produce a soft fluidic actuator with no requirement for an external compressor. The artificial muscles are arranged to increase the pressure of the internal fluid while providing a backbone to produce bending motion. The internal fluid provides the proposed actuators with a compliant structure much like pneumatically-driven soft actuators. These actuators may be used for several applications where pneumatically-driven fluidic actuators are currently used.

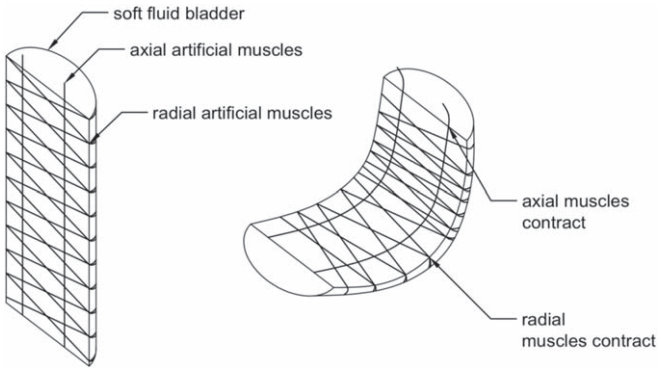

Figure 1. Depiction of actuator operation.

2. Materials and methods

The proposed actuator is made up of two main components, a sealed bladder filled with a compressible or incompressible fluid and an arrangement of nylon artificial muscles. The sealed bladder is made up of a soft deformable material and ideally takes a semi-cylindrical shape to maximize bending [12]. The flat component of the sealed bladder is then embedded with nylon artificial muscles. Furthermore, nylon artificial muscles are wrapped radially around the bladder as shown in figure 1. Similar to conventional bending fluidic actuators, the actuation path is dictated by the shape of the actuator and the relative difference in the Young's modulus of the two materials [13]. Bending is achieved when the artificial muscles activate. When activated, the artificial muscles contract which cause the fluid pressure in the sealed bladder to increase. This increased pressure creates a force which acts to expand the actuator axially. The axially arranged artificial muscles prevent axial extension and instead impose a bending motion in the actuator.

A prototype was fabricated to demonstrate the feasibility and performance of the proposed actuator design. The nylon artificial muscles were created from silver coated Nylon 6, 6 sewing thread. The conductive silver coating allowed for joule heating to be used for activation [14]. The fibres were coiled using a dc motor while a 200 g weight hung from the end of the fibre. The coils were then stretched by 30% and placed into an oven at 200 °C for 60 min [15]. This heat treatment is used to anneal the fibres, relieving stresses induced by the coiling process [15].

The silicone structure was created using Silicone TC-5005 (BJB Enterprises, Inc.), because it provides a soft compliant surface in addition to high elongation, and high tear resistance [16]. The actuator was prepared using two negative molds created from ABS plastic using a Stratysis 3D printer as seen

in figure 2. A liquid silicone pre-polymer was then poured into the molds to produce the final structure. After pouring the prepared silicone in the mold, it was left to cure at room temperature for 18 hours. The silicone was removed from the molds without any visible residue.

After removing the silicone from the molds, the structure was wrapped by hand, radially with nylon artificial muscles. The actuator was equipped with pressure and temperature sensor and sealed with a gasket mount (Figure 3).

3. Results

To characterize the performance of the proposed actuator, a number of experiments were conducted to measure the actuator's generated internal pressure, bending trajectory and torque at the actuator tip. To enable the robotics research community to utilize the proposed actuator, analytical models were formulated to predict the actuator's quasi-static behavior and validated against the experimental results. This provides robotics designers with information on the actuator's performance prior to manufacturing. The variables in the models were the nylon thermo-electric properties, the actuator dimensions, and the material properties of the silicone bladder.

When the nylon actuators contract, the actuator radius is decreased while the length of the actuator is constrained by the axially arranged nylon. As a result, the internal volume of the actuator decreases and the internal fluid pressure in the actuator increases. The increased internal pressure causes the actuator to bend to the desired configuration. Using the nylon thermo-electric model and the silicone material model, an analytical model was created to relate the nylon contraction to the internal fluid pressure.

The thermo-mechanical model for silver coated nylon actuators was characterized in previous research. The forces generated by the nylon muscles can be modelled as [15, 17]:

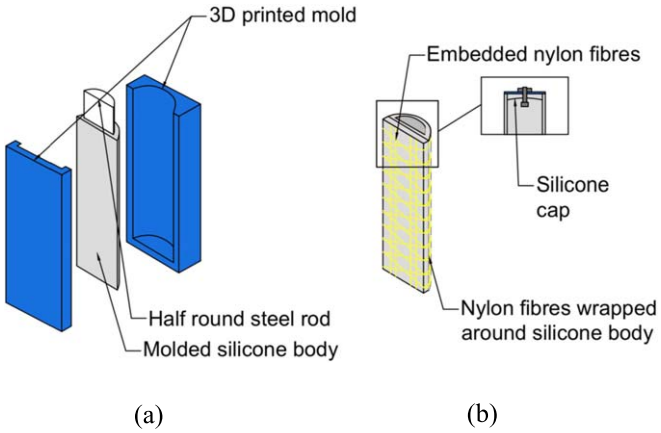

Figure 2. Depiction of the soft actuator fabrication process. (a) Molding the actuator body using a 3D printed part. (b) The nylon strain limiting layer is attached to the flat face of the actuator. Nylon is wound along the entire length of the actuator. The steel rod is removed from the silicone body and the ends are closed off with silicone. One end is sealed with a vented screw connected to a pressure sensor to measure the internal air pressure in the actuator.

Figure 3. Fabricated actuator. (a) Silicone actuator after removed from the mold. (b) Silicone actuator wrapped in nylon artificial muscles.

$$F = k(x - x_0) + b\dot{x} + c(T - T_0) \tag{1}$$

where F is the force generated by the nylon, x is the displacement at the end of the fiber, T is the temperature, and k, c, and b are constants determined from calibration.

The tensile stroke is defined as the amount of contraction exhibited by the muscles when activated. Kinzaid *et al* showed that the tensile stroke is a function of the wire temperature and is independent of the load applied if the stress in the wire remains below the tensile strength [17]. Sharafi *et al* showed that the tensile actuation is a function of the temperature of the wire and the coil geometry. This relationship can be modelled as [18]:

$$\varepsilon = \alpha - \gamma T - \beta \cdot \mathrm{erf}\left(\frac{T - T_g}{\sigma_g \cdot \sqrt{2}}\right) \tag{2}$$

where ε is the tensile stroke, T is the temperature of the wire, T_g is the glass transition temperature of the nylon, and α, γ, and β are constants determined by the spring coil index.

The nylon is plated with silver that allows it to conduct current. The silver creates a non-negligible resistance along the length of the nylon which was measured to be 0.15 Ω mm^{-1}. When a voltage is applied Joule heating occurs at causes the temperature of the wire to increase. Previous research has shown that a simple thermo electric model can be used to characterize the actuator temperature. This model is defined as [9]:

$$C\frac{dT}{dt} = \frac{V^2}{R} - \Lambda(T - T_{amb}) \tag{3}$$

where C is the thermal mass of the nylon, V is the applied voltage, R is the resistance of the nylon, Λ is the absolute thermal conductivity of the actuator, T is the temperature of the nylon and T_{amb} is the ambient temperature. The absolute thermal conductivity will change depending on the size of the actuator, the nylon wrapping configuration and the environment the actuator is operating in.

The actuators were fabricated using Silicone TC-5005 from BJB Enterprises, which exhibits non-linear behavior during large mechanical deformations [19]. Previous studies have shown that an incompressible Ogden model can accurately predict the deformation behavior of Silicone TC-5005. The stretch ratio of silicone is defined as [20]:

$$\lambda_i = \frac{x_i}{X_i} \tag{4}$$

where λ_i is the stretch ratio in the ith direction, x_i is the final length, and X_i is the original length in the ith direction. The strain energy density function is then determined as a function of the stretch ratios. This can be modelled as [20]:

$$W = \sum_{i}^{N} \frac{\mu_i}{\alpha_i}(\lambda_1^{\alpha_i} + \lambda_2^{\alpha_i} + \lambda_3^{\alpha_i} - 3) \tag{5}$$

where W is the strain energy density, λ_i is the stretch ratio in the ith direction, α_i and μ_i are Ogden parameters, and N represents the degree of the model used. For TC5005, N = 2 gives the best results [20]. The Cauchy stress can then be obtained by taking the derivative of the strain energy density function as [20]: .

$$\sigma_i = p + \lambda_i \frac{\partial W}{\partial \lambda_i} \tag{6}$$

where σ_i is the Cauchy stress, p is the hydrostatic pressure, λ_i is the stretch ratio in the ith direction, and W is the strain energy density.

The actuator design described above uses air as the internal fluid. For air at room temperature or above and atmospheric pressure, the ideal gas law can be used to relate the volume change to pressure change. Assuming constant temperature, the change in volume of the internal chamber can be related to the pressure using Boyle's law. This can be modelled as:

$$P_2 = P_1 \frac{V_1}{V_2} \tag{7}$$

where P_1 and V_1 are the initial pressure and volume in the chamber, while P_2 and V_2 are the pressure and volume in the chamber during actuation.

The volume of the internal chamber is compressed by the tensile contraction of the nylon and can be calculated as shown in equation (8). The actuator is constrained in the axial direction. As a result, it is assumed that the length of the actuator remains constant during the nylon contraction. Per the nylon thermo-electric model, the nylon tensile stroke is related to the wire temperature. This tensile stroke can also be related to the volume change as shown above.

$$\frac{V_1}{V_2} = \frac{1}{(1 - \varepsilon)^2} \tag{8}$$

where ε is tensile stroke in the nylon described by equation (1).

According to the nylon thermo-electric model, the nylon tensile stroke is a function of temperature, but remains constant with increasing stress up to the tensile strength [21]. Using the silicone material model, and the internal pressure model derived above, the stress in the nylon can be calculated to verify that it remains below the maximum tensile strength.

To calculate the stress in the nylon, a force balance was conducted between the internal pressure in the actuator, the material stress in the silicone, and the tensile stress in the nylon.

$$\sigma_n A_n n_{coils} = \int P \, dA + \int S_\theta dA_s \tag{9}$$

where σ_n is the stress in the nylon, A_n is the cross-sectional area of the nylon, n_{coils} is the number of nylon coils around the actuator, P is the internal pressure, S_θ is the principal stress in the circumferential direction.

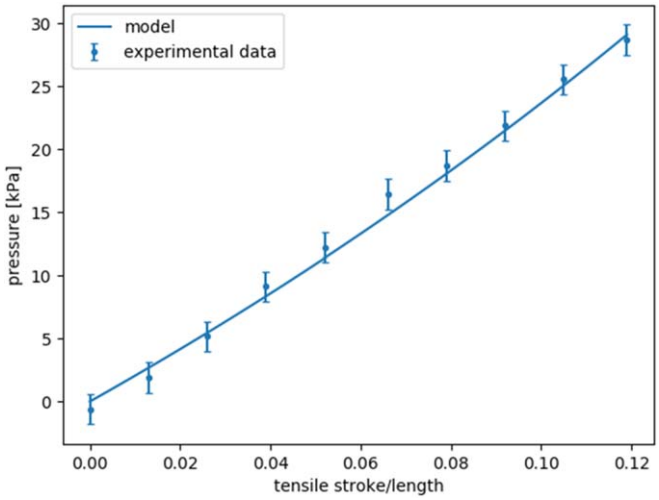

Figure 4. Internal pressure versus nylon tensile stroke plotted against the analytics model.

The material stresses can be calculated using the Ogden model shown above. The three principal stresses exist in the radial, circumferential, and axial directions. The stretch ratios in the axial and circumferential direction can be found based on the tensile stroke of the nylon. Assuming that the silicone is incompressible [20], the stretch ratios can be found as follows.

$$\lambda_l = 1 - \varepsilon \tag{10}$$

$$\lambda_\theta = 1 - \varepsilon \tag{11}$$

$$\lambda_r = \frac{1}{\lambda_l \lambda_\theta} \tag{12}$$

where λ_l, λ_θ, and λ_r represent the stretch ratios in the axial, circumferential, and radial directions, respectively. ε represents the nylon tensile stroke.

Experiments were conducted to verify the internal pressure model. Three variations of the actuator were fabricated and each was tested four times by applying a voltage to the nylon. The temperature of the nylon was measured and related to the nylon tensile stroke using equation (2) [18]. Figure 4 shows the relation between the nylon tensile stroke and the actuator internal pressure. Good correlation between the theoretical and experimental results was observed, demonstrating the validity of equation (8).

Based on the work of Polygerinos *et al* in [12], an analytical model was developed that captures the relationship between the internal pressure in the actuator and the actuator bending angle. Polygerinos *et al* showed that the internal pressure in the actuator and the stress in the actuator materials resulted in opposing bending moments as shown in equation (13)

$$M_a = M_\theta \tag{13}$$

where M_a represents moments produced by the internal pressure and M_θ represents the bending moment produced by the material stresses. The moment produced by the internal pressure can be calculated as:

$$M_a = 2(P_1 - P_{atm}) \int_{\pi/2}^{0} (a \sin \phi b) a^2 \cos^2 \phi \, d\phi \tag{14}$$

where P_1 is the internal pressure, P_{atm} is the atmospheric pressure, a, b and ϕ are shown in figure 5. The moments generated by the material stresses can be found by evaluating equation (14).

$$M_\theta = \int_0^b S_\beta (2a + t) L_\beta d\beta + 2 \int_{A_m} S_{\tau,\phi} ((a + \tau)^2 \sin \phi + b(a + \tau) L \, d\phi) d\tau \tag{15}$$

where M_θ is the moment generated by the material stress, S_B is the material stress in the base of the actuator and $S_{\tau,\phi}$ is the stress in the hemi-cylindrical section of the actuator. The material stresses are calculated using equation (5). An analytical solution could not be derived for equation (15) so it was solved numerically.

Six variations of the actuator design were fabricated and tested to verify the position model. Each actuator was tested four times by applying a range of voltages to the nylon wires while the motion of the actuator was recorded.

The position was later determined in the post processing step using the colour marker attached to the end of the actuator.

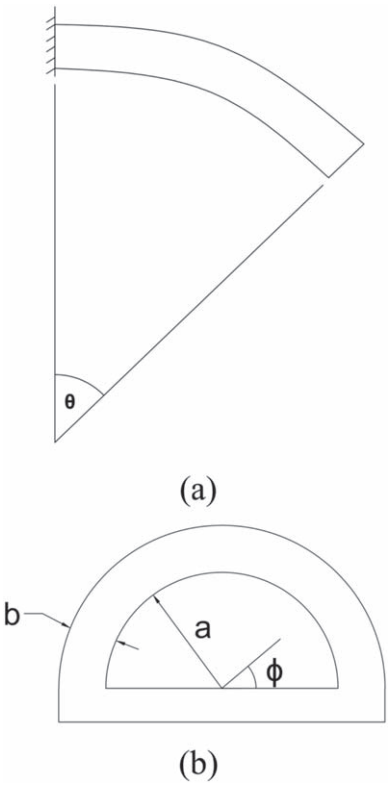

Figure 5. (a) The measured actuator bending angle (b) a cross section view of the actuator with labelled dimensions.

The bending trajectories of the actuator compared to the analytical models are illustrated in figure 6. A close correlation can be observed between the theoretical model and the experimental data. A maximum displacement error of 4.2% was calculated demonstrating the validity of the models. Small discrepancies can be seen in the pressure values due to initial prebending and gravitational influences. This resulted in a pressure error of 8.3%.

The analytical model derived in equation (15) can be extended to produce an expression for the actuator force. If the actuator is constrained to a zero-bending angle, no internal bending moments are generated during pressurizations. Therefore, the torque from the actuator base can be calculated as follows [12]:

$$M_f = FL_f = M_a = \frac{(4a^3 + 3\pi a^2 b)}{6} P_{in} \tag{16}$$

where F is the contact force at the actuator tip, L_f is the actuator length, and M_f is the external bending torque generated by the contact force around the actuator base. This equation describes the relationship between pressure and force under a constant bending angle [12]. Although equation (16) is only applicable for a bending angle of zero degrees, it follows that under constant pressure, the force output will decrease as the bending angle increases. This is due to the fact that larger moments are required to bend the actuator. Therefore, equation (16) defines the maximum force output for a given input pressure.

To verify the force model, experimental results were obtained by examining six variations of the actuator design. A range of voltages was applied to the nylon actuators and the force was measured at the actuator tip as shown in figure 7(a). The top layer of the actuator was fixed to prevent the actuator from bending during pressurization. The results are shown in figures 7(b)–(d). The experimental results show a close correlation with the predicted force at the tip of the actuator for this configuration.

Using the analytical model developed above, a position controller was developed to demonstrate the simplicity at which the proposed actuator may be controlled. A feedback control loop with an angle filter, as shown in figure 8, was implemented to demonstrate the ability of the analytical model of equation (15) to use pressure information to estimate bending angle in real time. Although the input to the system is voltage, the variation in the size of the actuator, and the ambient temperature affects the heating and cooling rate of the nylon. As a result, voltage provides an unreliable input to the feedback controller. Alternatively, the internal air pressure is relatively simple to measure in real time and is a good predictor of the actuator bending angle as shown in figure 6. In addition, utilizing pressure as the input to the feedback control loop, makes the controller

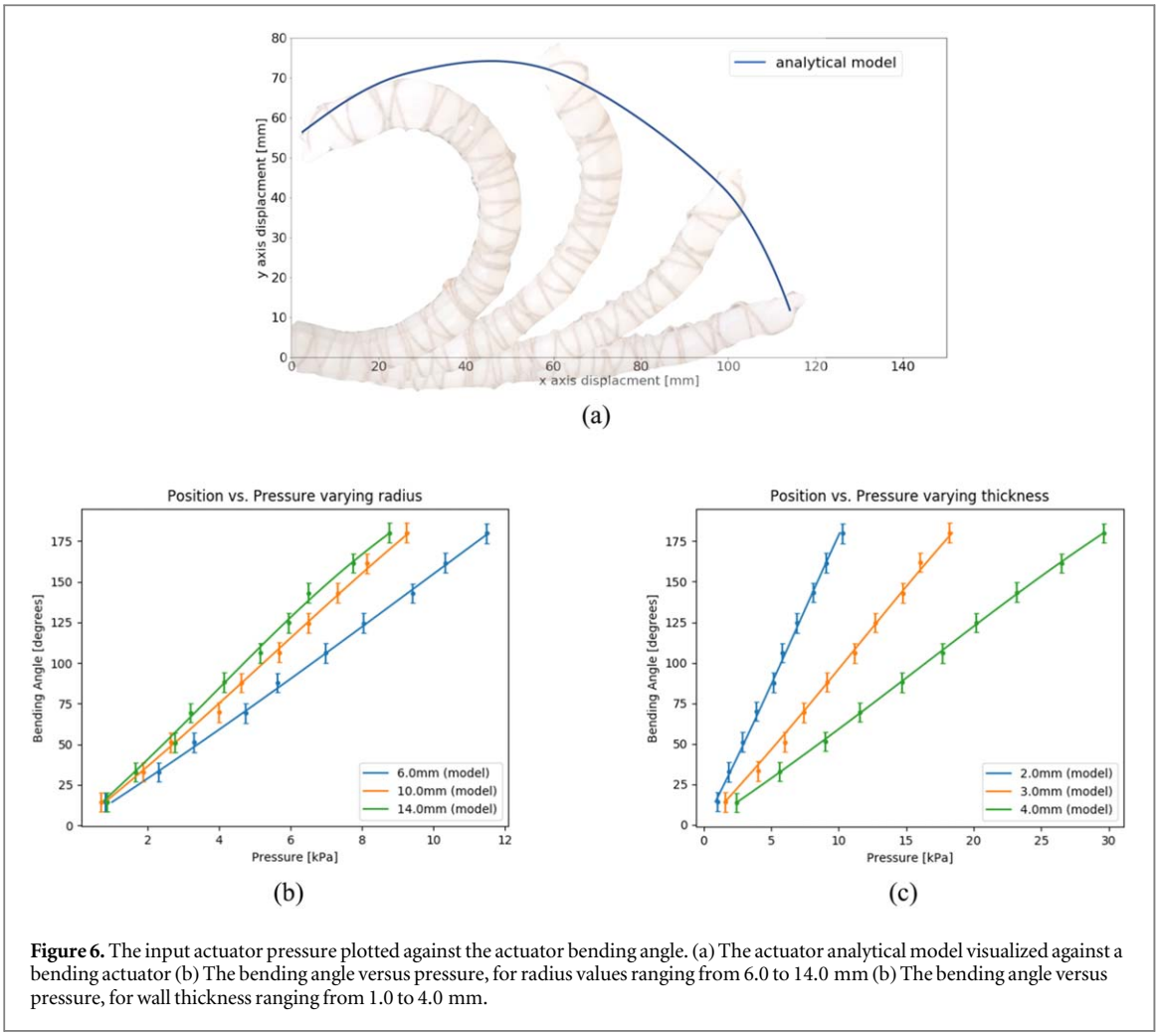

Figure 6. The input actuator pressure plotted against the actuator bending angle. (a) The actuator analytical model visualized against a bending actuator (b) The bending angle versus pressure, for radius values ranging from 6.0 to 14.0 mm (b) The bending angle versus pressure, for wall thickness ranging from 1.0 to 4.0 mm.

more versatile as it can be used in more operating environments. To control the power input to the nylon, a simple bang bang controller was utilized due to the the slow cooling rate of the actuator.

The feedback control loop was tested against a sinusoidal reference angle and a step response reference angle. The controller was successful in tracking an angle signal of 0.04 Hz as shown in figure 9. The maximum applied power to the actuator was 1.92 W (12 V, 160 mA). A larger power input could also be used which would reduce the actuator heating times, however, the cooling time is limited by the natural convection.

In order to provide evidence of the potential ability of the soft actuator to be used in robotic applications, a prototype of a soft robotic gripper (figure 10(b)) was constructed. Three actuators were mounted in a holding structure fabricated in ABS via a 3D printer. The gripper was powered by a single 9 V battery and with each actuator drawing approximately 130 mA of current. Figure 10(a) shows the pressure in the actuators during the grasping motion. Figure 10(b) shows the gripper grasping a ping pong ball through all stages of grapsing. Figure 10(c) shows that the gripper was able to grasp various objects. Each actuator could be manipulated individually, and there was no noticeable crosstalk between actuators caused by convective heating. Since the gripper is made out of a soft polymer and the actuation system is soft there is potential for this system to grasp delicate objects as similar configurations have demonstrated this capability [21–25].

4. Design considerations

The proposed fluidic actuator may be suitable for applications where pressure driven actuators are currently used. However, the size and forces generated by the actuator are limited by the capabilities of the nylon artificial muscles. It is important for the robotics designer to understand how these limitations affect the actuator's capabilities. Using the models developed above, a set of theoretical limits could be calculated based on the physical dimensions of the actuator to establish the maximum achievable torques and maximum actuator dimensions for a full range of motion.

According to equation (7), the stress in the nylon is proportional to the forces generated by the internal pressure and material stresses in the actuator walls. Furthermore, the nylon tensile stroke is a function of the

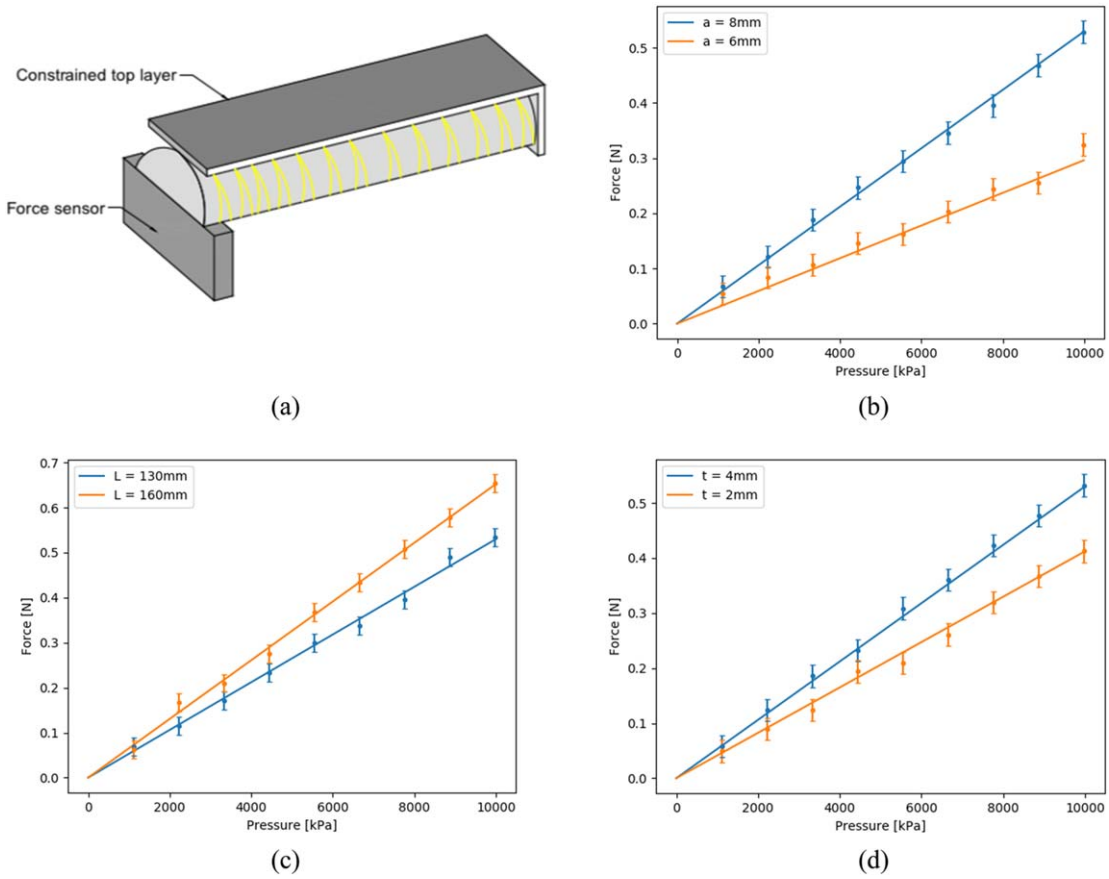

Figure 7. Force measurements of the actuator with various actuator dimensions. (a) Actuator force measured with the top layer constrained. (b) Actuator force versus internal pressure for various radii. (c) Actuator forces versus internal pressure for various actuator lengths. (d) Actuator force versus pressure for various wall thicknesses.

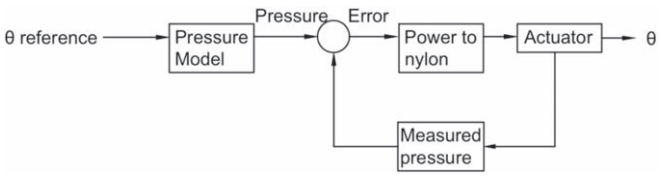

Figure 8. Schematic of the closed loop controller for actuator bending angle.

temperature only and is independent of the tensile stress as long as the tensile stress remains below the ultimate tensile strength of the nylon [17]. Using the tensile stroke, the internal pressure in the actuator can be calculated using equation (9) and the material stresses in the actuator can be calculated using equation (13). Based on the calculated pressure and material stresses, the stress in the nylon can be calculated using equation (9). It is assumed that this force is evenly distributed over the number of nylon coils which can be calculated based on the wrapping angle (Figure 11) and the width of the nylon. The force in the nylon is then checked to remain below the ultimate tensile strength. Furthermore, Haines *et al* showed that the nylon ultimate tensile strength and the tensile stroke is dependent on the nylon coil index and that an inverse relationship exists between the nylon ultimate tensile strength and the maximum tensile stroke. The results are summarized in figure 12(a).

Figure 12(a) shows how the actuator dimensions affect the tensile force generated in the nylon. As the actuator dimensions increase, the force required to compress the actuator walls increases beyond the maximum capabilities of the nylon. The nylon limitations for various coil indices are shown with a dashed black line.

Using the results of figure 12(a), the maximum achievable torque for a proposed actuator can be calculated given the actuator dimensions and the nylon coil index (equation (14)). The nylon thresholds for various wrapping angles were determined using equation (9) and are shown as a dashed black line. From figure 12(b) it can be observed that a larger coil index produces a larger torque for smaller actuator dimensions. However, as

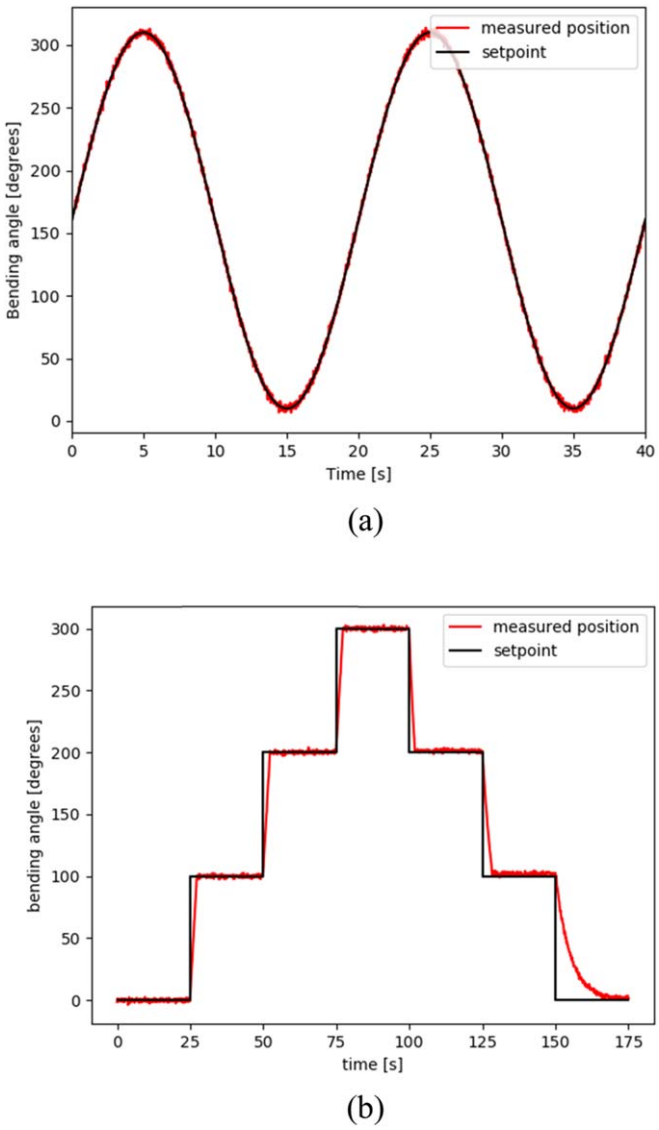

Figure 9. Feedback control loop performance. (a) Actuator tracking a sinusoidal reference angle with a period of 0.04 Hz (b) Step response of the actuator controller.

the actuator dimensions increase, the nylon quickly reaches its limitations. In addition, by increasing the wrapping angle, the expansion force generated by the internal pressure and materials stresses is distributed over less nylon coils. As a result, the maximum force in the nylon is reached sooner for actuators of the same dimensions.

Figure 12(c) summarizes the theoretical limits for the bending angle of the proposed actuator. The bending angle was calculated using equations (13) and (9) was used to determine the bending angle limitations. Given an actuator and its dimensions, using figure 12(c) the designer can determine if the actuator can undergo a full range of motion. As the actuator dimensions increase, the stress in the nylon increases causing the range of motion to decrease. Similar to the maximum torque, by increasing the wrapping angle, the expansion force generated by the internal pressure and materials stresses is distributed over less nylon coils. As a result, the maximum force in the nylon is reached sooner for actuators of the same dimensions.

Using the results of figure 12, a robotics designer with higher force requirements might consider using the maximum radius 20 mm with a nylon coil index of 1.1 (figure 12(b)). The designer could select a large but reasonable wall thickness of 6 mm and a length of 90 mm. According to figure 12(b), this actuator could produce a maximum force of 1.2 N. The resulting actuator could also undergo a full range of motion according to figure 12(c).

On the contrary, another robotics application may have smaller force requirements but the actuator is space constraint. An actuator with a radius of 7.5 mm, length of 70 mm and a wall thickness of 2 mm can produce a maximum force of 0.15 N if nylon with a coil index of 1.7 is used.

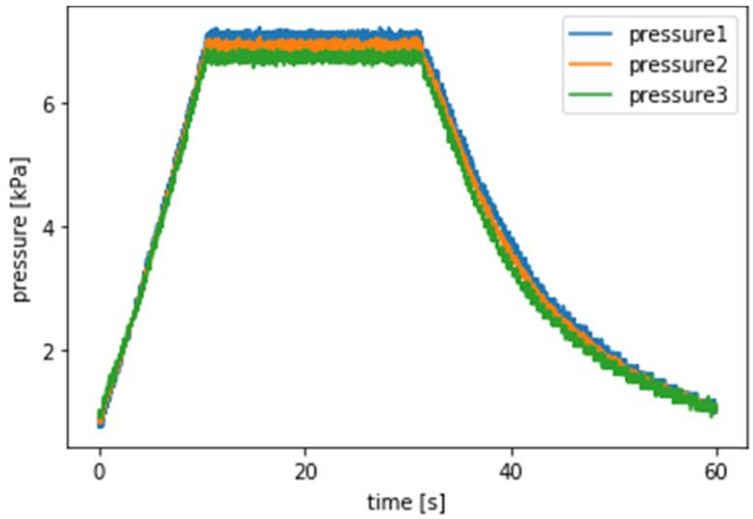

(a)

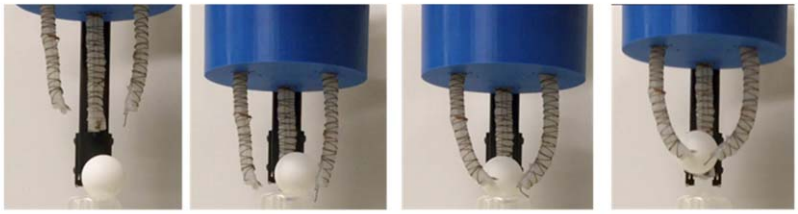

(b)

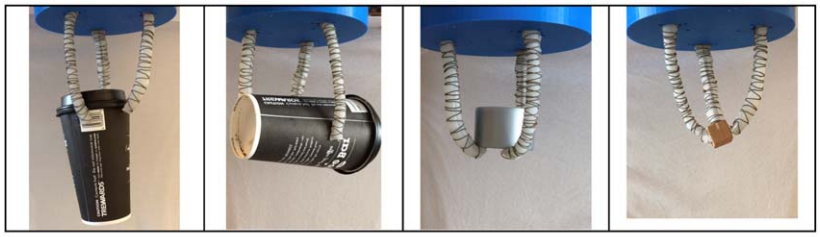

(c)

Figure 10. Soft gripper demonstration. (a) Plot of pressure versus time for the actuators in the gripper. (b) The soft gripper shown grasping a ping pong ball through all stages of grasping (c) The soft gripper shown grasping various objects.

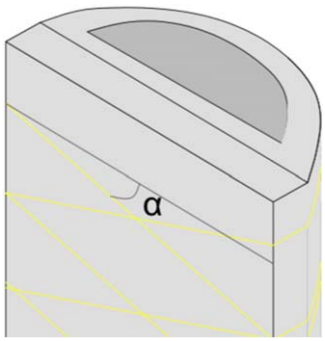

Figure 11. Depiction of the nylon wrapping angle α.

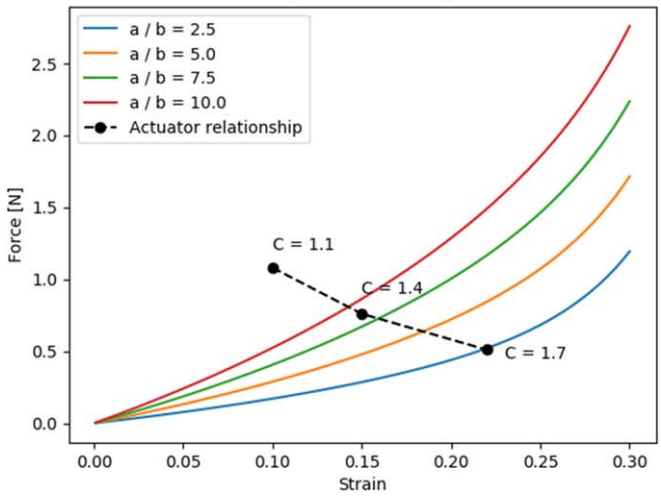

(a)

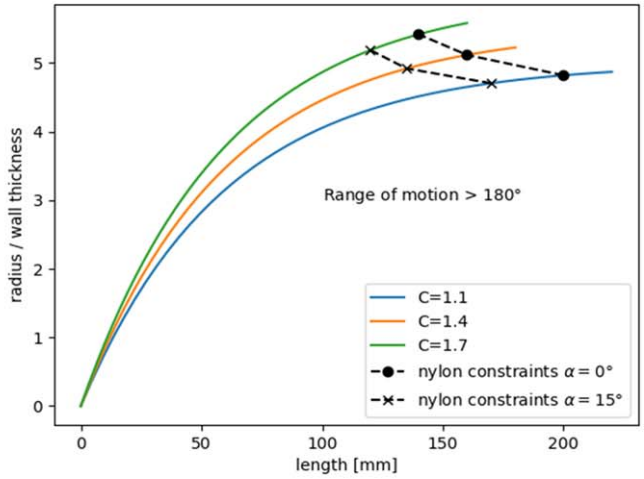

(b)

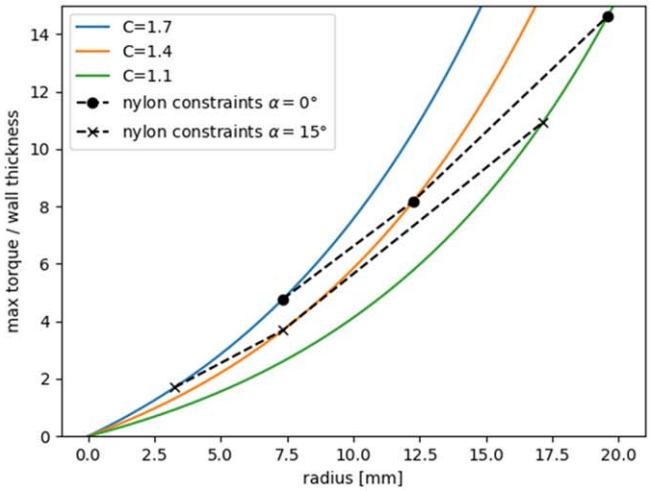

(c)

Figure 12. (a) Forces in the nylon versus tensile stroke for various actuator dimensions. (b) Maximum achievable torques for versus actuator dimensions. Actuator limitations shown as a dashed black line for various wrapping angles (c) Maximum achievable range of motion versus actuator dimensions. Actuator limitations shown as a black dashed line for various wrapping angles.

5. Discussion and conclusion

Soft fluidic actuators can generate complex motions at a low mechanical cost with simple controllers. To date, the development of such actuators has largely relied on mechanical compressors or pumps to supply the input fluid pressure. The proposed actuator aims to bridge the gap between current fluidic actuators and a complete, compact, soft solution. By utilizing nylon actuators, the proposed fluidic actuator has no need for an external compressor or pump while still providing the benefits of a soft, compliant fluid actuator.

Depending on the application, the proposed actuators could be used with off the shelf batteries or commercially available flexible batteries to produce a completely soft portable system. For example, the gripper described above in figure 10 used a 9 V battery and drew approximately 400 mA of current at maximum capacity. Flexible batteries such as those avaible from Jenax Inc. [26] could have been used for limitted amounts of time. In contrast, conventional bending fluidic actuators require both a compressor and an electrical system. Although the electrical system can be made portable or flexible, soft portable compressors are not currently available [1]. For the robotics designer looking for portable soft robotics system, the proposed actuators could potentially be suitable.

For robotics designers looking to utilize the proposed actuators, analytical models were developed to provide performance information on the actuator prior to manufacturing. The position model showed a close correlation with the experimental data. A maximum displacement error of 4.2% was calculated demonstrating the accuracy of the models. The small discrepancies were likely due to the initial bending of the actuator caused by gravitational influences. Additionally, the force model showed good correlation with the experimental results (maximum force error of 4.3%). Using the analytical models, a minimalist position controller was implemented to demonstrate how a designer might implement a control system in practice. The analytical models were also used to calculate a set of design considerations for the robotics engineer. These design plots can be used select the optimal nylon fibre and actuator dimensions to best suit the designer's requirements.

Nylon actuators offer a lightweight alternative solution to traditional actuation methods. Currently the system is limited by restricted muscle relaxation time. Thus, further research could be conducted to improve the speed of cooling the nylon. This could be done by immersing the coils in water, increasing air flow around the wire, adding heat sinks to the design, or decreasing the air temperature around the coils. Additionally, this problem could be overcome by adding opposing actuators that could compensate for the slow relaxation times. The wrapping procedure could also be improved. Currently the nylon is wrapped radially by hand as this was a preliminary research project.

However, the procedure could be improved by creating an automated system. The system could rotate the silicone bladder while moving along the axis. The coiled nylon could be fed and wrapped around the bladder as it rotates. This could improve the reliability of the proposed actuators by reducing the bulging effect and potential twisting induced caused by wrapping the actuators manually.

Research in the area of soft robotics is an emerging field and nylon actuators could potentially provide a soft, lightweight, alternative to pressure driven fluidic actuators. By combining the nylon actuators with flexible power sources future studies may examine how robots can be composed of entirely soft components and remain completely self-contained.

ORCID iDs

Lee Sutton https://orcid.org/0000-0003-0990-1289

References

[1] Rus D and Tolley M T 2015 'Design, fabrication and control of soft robots *Nature* **521** 467–75
[2] Madden J D *et al* 2004 Artificial muscle technology: physical principles and naval prospects *IEEE J. Oceanic Eng.* **29** 706–28
[3] Wehner M *et al* 2014 Pneumatic energy sources for autonomous and wearable soft robotics *Soft Robotics* **1** 263–74
[4] Burgar C G 2000 Development of robots for rehabilitation therapy: the Palo Alto VA/Stanford experience *Journal of Rehabilitation Research and Development* **37** 663–674
[5] Bar-Cohen Y 2000 'Electroactive polymers as artificial muscles: capabilities, potentials and challenges *Robotics 2000* (New Mexico: Albuquerque)
[6] Fremond M 1996 *Shape Memory Alloy: A Thermomechanical Macroscopic Theory* (Vienna: Springer Vienna)
[7] Moein H and Menon C 2014 'An active compression bandage based on shape memory alloys: a preliminary investigation *Biomedical Engineering Online* **13** 135
[8] Huang W 2002 'On the selection of shape memory alloys for actuators *Mater. Des.* **23** 11–9
[9] Yip M and Gunter N 2015 'High-performance robotic muscles from conductive Nylon Sewing thread *2015 IEEE Int. Conf. on Robotics and Automation (Seattle, Washington)*
[10] Otsuka K and Wayman C M 1999 *Shape Memory Materials* (London: Cambridge University Press)
[11] Haines C 2014 Artificial muscles from fishing line and sewing thread *Science* **343** 868–72

[12] Polygerinos P, Wang Z, Overvelde J T, Galloway K C, Wood R J, Bertoldi K and Walsh C J 2016 'Modeling of soft fiber-reinforced bending actuators *MODELING of Soft Fiber-Reinforced Bending Actuators* **31** 778–89
[13] Chang B *et al* 2012 A spatial bending fluidic actuator: fabrication and quasi-static characteristics *Smart Mater. Struct.* **21**
[14] Mirvakili S, Rafie A, Hunter I, Haines C S, Li N, Foroughi J, Naficy S, Spinks, Geoffrey M B and Madden J D 2014 Simple and strong: twisted silver painted nylon artificial muscle actuated by Joule heating *International Society for Optics and Photonics, 2014* **9056** 9056I
[15] Sutton L, Moein H, Rafiee A, Madden J D and Menon C 2016 Design of an assistive wrist orthosis using conductive nylon actuators *Biomedical Robotics and Biomechatronics (BioRob)* (Singapore)
[16] Chang B 2011 *Quasi-Static Analysis and Control of Planer and Spatial Bending Fluidic Actuator* (Burnaby, British Columbia, Canada: Simon Fraser University)
[17] Kianzad S A, Ko F, Spinks G M and Madden J D 2015 'Nylon coil actuator operating temperature range and stiffness *PIE Smart Structures and Materials + Nondestructive Evaluation and Health Monitoring*
[18] Sharafi S and Li G 2015 'A multiscale approach for modeling actuation response of polymeric artificial muscles *Soft matter* **11** 3833–43
[19] Kianzad S *et al* 2015 Nylon coil actuator operating temperature range and stiffness *SPIE Smart Structures and Materials + Nondestructive Evaluation and Health Monitoring*
[20] Ahmadi S 2013 Fabrication and electromechanical examination of a spherical dielectric elastomer actuator *Smart Mater. Struct.* **22** 115004
[21] Manti T 2015 A novel type of compliant underactuated robotic hand for grasping *Soft Robotics* **35** 161–85
[22] Soft Robotics Inc. 2019 [Online]. Available: https://softroboticsinc.com [Accessed 11]
[23] Wei Y 2016 A novel variable stiffness robotic gripper base on integrated soft actuatoring and particle jamming *Soft Robotics* **3** 134–43
[24] Brock R 2016 A novel type of compliant underactuated robotic hand for dexterous grasping *Internal Journal of Robotics Research* **35** 107–16
[25] Hirai Z 2016 A 3D printed soft gripper integrated with a curvature sensor for studying soft grasping *IEEE Internation Symp. on System Integration*
[26] Jenax Incorporated Jenax battery products Jenax Incorporated, [Online]. Available: https://jenaxinc.com/ Accessed 23 January 2019